Ultrasonics Sonochemistry 92 (2023) 106251

Contents lists available at ScienceDirect

Ultrasonics Sonochemistry

journal homepage: www.elsevier.com/locate/ultson

Sonochemical construction of hierarchical strontium doped lanthanum trisulfide electrocatalyst: An efficient electrode for highly sensitive detection of ecological pollutant in food and water

Umamaheswari Rajaji [a], K. Yogesh Kumar [b], Rameshkumar Arumugam [c,d], Asma A. Alothman [e], Mohamed Ouladsmane [e], Ren-Jei Chung [f,*], Ting-Yu Liu [a,g,h,*]

[a] Department of Materials Engineering, Ming Chi University of Technology, New Taipei City 243303, Taiwan
[b] Department of Chemistry, Faculty of Engineering and Technology, Jain University, Bangalore 562112, India
[c] Department of Chemistry, Bannari Amman Institute of Technology, Sathyamangalam, Erode, India
[d] Korea University of Technology and Education, Cheonan-si 31253, Chungcheongnam-do, Republic of Korea
[e] Department of Chemistry, College of Science, King Saud University, Riyadh 11451, Saudi Arabia
[f] Department of Chemical Engineering and Biotechnology, National Taipei University of Technology (Taipei Tech), Taipei 10608, Taiwan
[g] Research Center for Intelligent Medical Devices, Center for Plasma and Thin Film Technologies, Ming Chi University of Technology, New Taipei City 243303, Taiwan
[h] Department of Chemical Engineering and Materials Science, Yuan Ze University, Taoyuan City 32003, Taiwan

ARTICLE INFO

Keywords:
Sonochemical synthesis
Metal doped lanthanum sulfide
Toxic herbicide detection
Mesotrione determination
Water pollutant detection
Food pollutant detection

ABSTRACT

Herbicides are used constantly in agriculture to enhance productivity across the globe. This herbicide monitoring requires utmost importance since its high dose leads to ecological imbalance and a negative impact on the environment. Moreover, a quantification of toxic herbicide is one of the important problems in the food analysis. In this work, deals with the development of a simple, and facile one-pot sonochemical synthesis of strontium doped La_2S_3 ($Sr@La_2S_3$). Morphological and structural characterization confirms the doping of $Sr@La_2S_3$ to generate a hierarchical layered structure. The electrochemical performance of modified with rotating disk electrode (RDE) using $Sr@La_2S_3$ composite is high, compared to La_2S_3 and bare electrodes towards the quantitative detection of mesotrione (MTO) in phosphate buffer. $Sr@La_2S_3$/RDE showed good sensitivity for MTO detection and it exhibit a range of 0.01–307.01 μM and limit of detection of 2.4 nM. Besides, the selectivity of fabricated electrode is high as it can electrochemically reduce MTO particularly, even in the presence of other chemicals, biological molecules and inorganic ions. The repeatability of MTO detection is high even after 30 days with a lower RSD values. Hence, simple fabrication of $Sr@La_2S_3$/RDE could be a novel electrode for the sensitive, selective, and reproducible determination of herbicides in real-time applications.

1. Introduction

Interestingly, the sonochemical approach has been proved to be a non-toxic method to obtain novel nanomaterials. The chemical effects of ultrasonic irradiation arise from acoustic cavitation and activation, in other words, the formation, growth and implosive collapse of bubbles in a chemical reaction medium, which results in a spontaneously high temperature and pressure pulse [1–3]. Based on this sonochemical reaction conditions of high pressure, temperature, and intense micromixing process attained during acoustic cavitation abilities lead to different and remarkable properties of nanomaterials in the irradiated reaction mixture [1,4]. Based on an environmental perspective, the sonochemical irradiation is one of the advantageous, because it could be utilized to facilely synthesize doped nanomaterials without using toxic reagents and chemicals [5]. To prepare an economical and eco-friendly nanomaterial, sonochemical approach may be among the best way as a synthesis direction.

Lanthanum sulfides are the class of rare-earth chalcogenides materials in various forms; LaS, La_2S_3, and La_3S_4. Among these, dilanthanum trisulfides (La_2S_3) is the stable one consists of both positive (La^{+3}) and negatively charged ions (S^{2-}). Lanthanum metal having a unique band structure due to the existence of f-orbital electrons, which can generate

* Corresponding authors at: (Prof. Ting-Yu Liu) Department of Materials Engineering, Ming Chi University of Technology, New Taipei City 243303, Taiwan and (Prof. Ren-Jei Chung) Department of Chemical Engineering and Biotechnology, National Taipei University of Technology (Taipei Tech), Taipei 10608, Taiwan.
E-mail addresses: rjchung@ntut.edu.tw (R.-J. Chung), tyliu0322@gmail.com, umachemist24@gmail.com (T.-Y. Liu).

https://doi.org/10.1016/j.ultsonch.2022.106251
Received 14 October 2022; Received in revised form 24 November 2022; Accepted 27 November 2022
Available online 28 November 2022

d-π coordination complexes with aromatic ring carbons [6]. Besides, the sulfide groups could easily form an electrostatic bond with the sensing analytes and along with this, it enhances the porous and hydrophilic nature. Compared to other metal-based sulfides, La_2S_3 seems less toxic and stable. La_2S_3 exhibits properties like good conductivity, variable oxidation state, enhanced surface area and ability to undergo redox reaction, it has been used as electrode materials in supercapacitors and water purification through adsorption and photocatalytic approach [7]. In additional, enhance the electrocatalytic performance of La_2S_3, it is more preferred to dope with other rare earth metals. Mainly, strontium (Sr) is one of the rare earth metals used as dopant to enhance electrocatalytic properties [8]. When Sr is doped to La_2S_3, there will be a generation of two cations with one sulfur anions. This doping of metal-to-metal sulfide will enhance the electrochemical performance by enhancing the electron mobility upon structural changes.

The properties of La_2S_3 depend on the structure, phase, crystallinity, shape etc. These properties are attributed to the synthetic approach used. La_2S_3 has been synthesized by thermal decomposition, spray pyrolysis, and sulphurization of oxide in presence of H_2S, successive ion layer adsorption and reactions methods [9,10]. All these methods involve one or the other ambiguities like the use of hazardous solvents, time-consuming, expensive, high-energy input etc. So there is a need of a simple, cost-effective method for the generation of $Sr@La_2S_3$ with good structural properties. Authors in the present work describe a simple, facile, and economical one-pot synthesis of Sr doped La_2S_3 by hydrothermal approach. At present, the population across the globe is increasing and is expected to reach 9 billion by the year 2050 [11]. Once there is an increase in the population the need for food production is to be raised by 75 to 90 % [11]. There are several issues related to crop production like weeds, animal pests, pathogens, crop management, and socioeconomic constraints. Weeds are the unwanted plants that show competition with crops for space, nutrients, water, sunlight and additionally act as hosts for the growth of several insects that harm the growth of crops [12,13]. Herbicides are the solution for the removal of unwanted weeds in the field due to its ease of application and economical since it saves labour cost. One of the triketone family herbicides used as selective weed control in maize, sugarcane, and rice is mesotrione (IUPAC name: 2-(4-methylsulphonyl-2-nitrobenzyl) cyclohexane-1,3-dione). Syngenta marketed mesotrione (MTO) in the year 2001 [14]. Due to the outstanding weed control property of MTO it is used to control the growth of broad leaves and weeds during their pre and its post-emergence [14]. Triple action formula is observed in MTO i. e. on roots, shoots as well as leaves. Main crops like Paddy, cane and maize are highly tolerant to MTO since they can metabolize the herbicide into inactive products. Like other herbicides, MTO could also be washed from leaves to soil and aquatic compartments [15]. Later accomplish in both surface and groundwater. Accumulation of MTO exhibits toxicity on non-target organisms and adversely disturbs the aquatic ecosystem by affecting the growth of microalgae. MTO and its metabolites are active to disturb the prokaryotic structures in water and lead to algal blooms as observed in the blue-green algae disaster that happened in 2007 which damaged the ecological unbalance [15]. Human beings are also affected even when a trace amount of MTO is consumed either in the form of food or water. Monitoring the MTO concentration in soil and water is of high importance as it falls under environmental remediation. Efficient, sensitive, selective, cost-effective, accurate and precise technique is needed for the detection of MTO.

Several analytical methods have been credited for the determination of MTO. The methods available for the detection of mesotrione are high-performance liquid chromatography (HPLC), gas-chromatography (GC), liquid chormatography-mass spectroscopy (LC-MS), colorimetric and diode array detectors [15–21]. These methods are sensitive but involve the use of hazardous reagents/solvents; time-consuming some may not be selective in detection. Hence, there is a need for selective as well as a sensitive method for the determination of MTO. Among several available new techniques for analysis, sensor-based techniques are of high priority. Among the different types of sensors available, florescent probe sensors, optical sensors, biosensors and etc [22,23], electrochemical sensors are well used for the sensitive determination of herbicides [18]. The main advantage of electrochemical sensors is simple, limited use of hazardous materials, quick, and low cost. Different electrodes used in electrochemical sensors are glassy carbon electrode, gold electrode, screen-printed carbon electrode, carbon paste electrode and etc [24–26]. When these electrodes are used as such, the high efficiency of the electrode will not be reached due to high overpotential, slow kinetics during the electrochemical process. Hence, modification of the electrodes is much needed for the sensitive detection of analytes. The material used to modify electrodes should be having superior electrical conductivity, rich redox centers on the surface, swift electrochemical reactions, exceptional electron/electrode interface, specific structural defects and etc [27–29]. Therefore, materials like metal oxides, metal sulfide, carbon materials, metal vanadate's, nanocomposites are used to modify electrodes could suit best for the electrochemical redox reactions for sensitive and selective analytical detection of analytes.

The characterization of $Sr@La_2S_3$ showed a hierarchical layered structure which is advantageous in electrochemical applications due to the easy mobility of electrons. The $Sr@La_2S_3$ modifier coated GCE showed an enhanced electrochemical sensing performance for the detection of mesotrione herbicide. The developed method is having good sensitivity, selectivity, stability along with practical applicability. The $Sr@La_2S_3$ could be developed as an alternative composite for the detection of herbicides, pharmaceuticals or other organic molecules that readily undergo redox reactions (Scheme 1).

2. Experimental

2.1. Materials and methods of the work

Mesotrione, lanthanum (III) nitrate hexahydrate, thioacetamide, strontium nitrate, and all other chemicals and reagents were collected from Sigma-Aldrich, Taiwan and used without further purification and washing process. The sonochemical synthesis was used by the probe of JY92-IIN Scientz (Xinzhi Co). Further, details of methods and instrumentation details were given in the supporting file.

2.2. Green based sonochemical synthesis of $Sr@La_2S_3$

In a synthesis of $Sr@La_2S_3$, the precursors 10 mM of strontium nitrate (ACS reagent, ≥99.0 %), 20 mM of lanthanum(III) nitrate hexahydrate (≥99.0 %), and 100 mM of sodium sulfide nonahydrate (ACS reagent, ≥98.0 %) were added into the 60 mL of deionized water. And then, the mixture was stirred homogeneous using magnetic stirrer at room temperature. After 10 min, the reaction solution was sonicated for 4 h. The ultrasonication process and reaction is conducted under optimum frequency at 50 kHz and optimum power at 200 W. After the reaction time, the obtained solution was centrifuged at 8000 RPM to collect the product and supernatant excess solution was discarded. At last, the resultant precipitate was filtered and washed with pure water and dried in a vacuum oven. Finally, the product was got after consecutively cleaned and dried process to obtain $Sr@La_2S_3$ material (Scheme 2).

2.3. Fabrication of $Sr@La_2S_2$ modified GCE/RDE

The working electrode; GCE/RDE has been modified using $Sr@La_2S_3$. First, the GCE/RDE was subjected to polishing using 0.05 μm alumina powder and sonicated in water. Two mg mL^{-1} of suspension was dispersed in deionized water through sonication, 8 μL of the suspension was drop casted on GCE/RDE and used after drying at 75 °C.

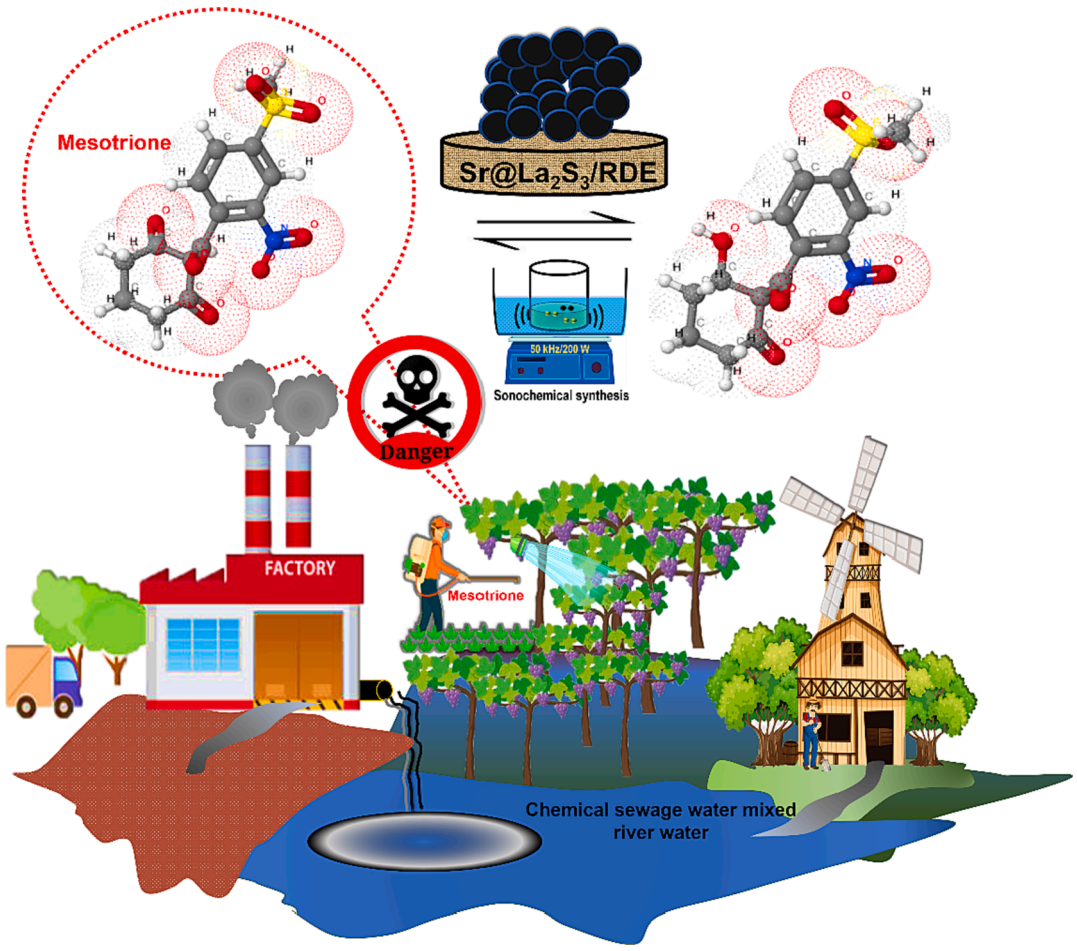

Scheme 1. Schematic representation for the electrochemical sensors and its electrocatalytic application.

3. Results and discussion

3.1. XRD and XPS analysis of Sr@La_2S_3 electrode material

The XRD spectrum of the Sr@La_2S_3 material is chemical and structural analysis in the 2θ range of 20° to 85° (Fig. 1A), which shows peaks with corresponding planes of (211), (321), (330), (212), (412), (610), (620), (213), and (209). The observed 2θ with corresponding XRD planes are well-matched with the ICSD card of 01–089–4035 and it's indicate successful crystallographic of tetragonal La_2S_3 [30]. Moreover, the peaks are appearing at 34° to 42° corresponds to the Sr (Xiaobin et al. 2021). Based on this data, the XRD analysis suggest that Sr has been doped with La_2S_3 particles at the prescribed conditions, and it act as a Sr@La_2S_3 nanomaterials [31,32].

XPS analysis was used to investigate the detailed surface elemental composition as well as the exact ionic states of the as-synthesised sample, and the resulting full survey spectrum is shown in Fig. 2A. The total survey spectrum clearly demonstrates the presence of La, Sr, S and O in the composites, and the results are consistent with the elemental results in Fig. 3I. The high resolution XPS spectrum of Sr 3d states is shown in Fig. 2B. Two resolved peaks at 133.3 eV and 135.1 eV belonging to Sr^{2+} $3d_{5/2}$ and $3d_{3/2}$, respectively are detected [33]. Fig. 2C depicts the XPS spectra of La, which mainly consist of the spin orbit splitting of La $3d_{5/2}$ and La 3d3/2. La $3d_{5/2}$ spectra, which contain two electronic transitions, the first of which is situated at about 837.6 eV and the second at 834.5 eV [34]. The peak at 835 eV is attributed to a satellite generated by a valence-band electron transitioning to an empty 4f orbital at the same time as a 3d electron transitioning to a continuum state. The binding of lanthanum to sulphur in La_2S_3 is responsible for these two peaks in the La $3d_{5/2}$ spectrum. In trivalent lanthanum compounds including halide, oxide, and sulphide, this sort of satellite structure has been seen frequently. The peaks of La $3d_{3/2}$ were located at 852.5 eV and 856.3 eV, clearly suggesting that La is in its La^{3+} oxidation state [6,7]. The same sample's S 2p core level XPS spectra revealed two significant peaks at 161.8 eV and 163.0 eV [35], corresponding to the S $2p_{3/2}$ and S $2p_{1/2}$ spin orbit splits which is in good agreement with the literature (Fig. 2D).

3.2. Morphological analysis of Sr@La_2S_3

Fig. 3A1, A2, and A3 represents the SEM images of Sr@La_2S_3 composite. In Fig. 3A2 shows the circular district strontium particles were accumulating on the flake surface of the La_2S_3. Fig. 3A3 reveals the exact structure of the composite at higher magnification. The TEM images of the composite were observed in Fig. 3B1, B2, and B3 at different magnifications. These TEM images shows the dark and light spots on the composite is due to different angle of orientation of the composite crystals. The HR-TEM image Fig. 3C show the different direction orientation of the fringes of the Sr@La_2S_3 composite and sample has a polycrystalline in nature. The fringes have distance of 321 nm, which is corresponds to the d spacing of the Sr and La_2S_3 in the XRD analysis. The SAED patterns of the Sr@La_2S_3 composite shown in Fig. 3D, the hkl values of the Sr@La_2S_3 composite were matched with the XRD values of corresponding d spacing of Fig. 1A the data gives the supporting evidence to the poly crystals of Sr@La_2S_3 composite. The elemental mapping of the Sr@La_2S_3 composite analysed in Fig. 3E, F and G, indicates the presence of Sr, La, and S respectively. The EDS spectra was showing the all the elements of the Sr@La_2S_3 composite were observed in the

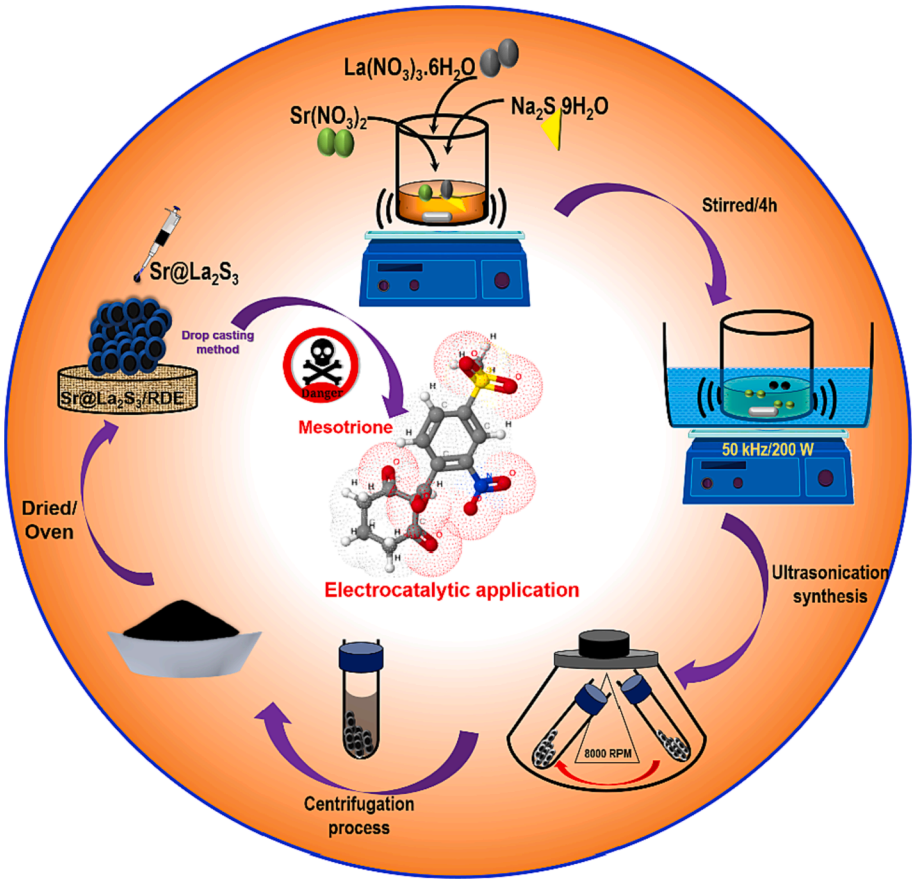

Scheme 2. Schematic representation for the synthesis of Sr@La_2S_3 catalyst.

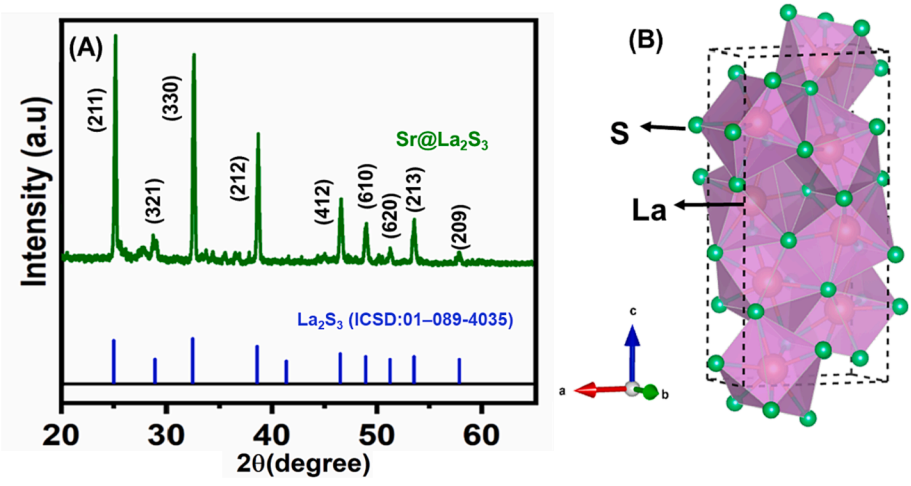

Fig. 1. (A) XRD pattern of $La_2S_3$and Sr@La_2S_3. (B) Crystal analysis of La_2S_3 particle.

Fig. 3H.

3.3. *Electrocatalytic activity of Sr@La_2S_3/GCE*

Electrochemical performance of the synthesized materials is mainly related to the reaction mechanism that is allied with electron and charge mobility. Electrochemical impedance spectroscopy (EIS) analysis has been used to understand the electrode-solution interface [36,37] and data is given in Fig. 4A. Nyquist plot of GCE, La_2S_2/GCE, and Sr@La_2S_3/GCE in 5 mM $[Fe(CN)_6)]^{3-/4-}$ having 0.1 M KCl shows different R_{ct} values due to the surface modification. The inset (Randle's circuit) of exhibits lower charge transfer resistance in Sr@La_2S_3/GCE (32.6 Ω) along with semi-circular nature when compared to La_2S_2/GCE. The electrochemical surface area of the Sr@La_2S_3/GCE was calculated using a Randles-Sevcik Eq. (1) [38–40]. The electrochemical active-surface area was calculated by using of the unmodified and modified electrodes (Fig. 4B and C).,

$$Ip = 2.69 \times 10^5 AD^{1/2}n^{3/2}v^{1/2}C \quad (1)$$

Herein, A, D, I_p, n, v, and C are representing the active surface area

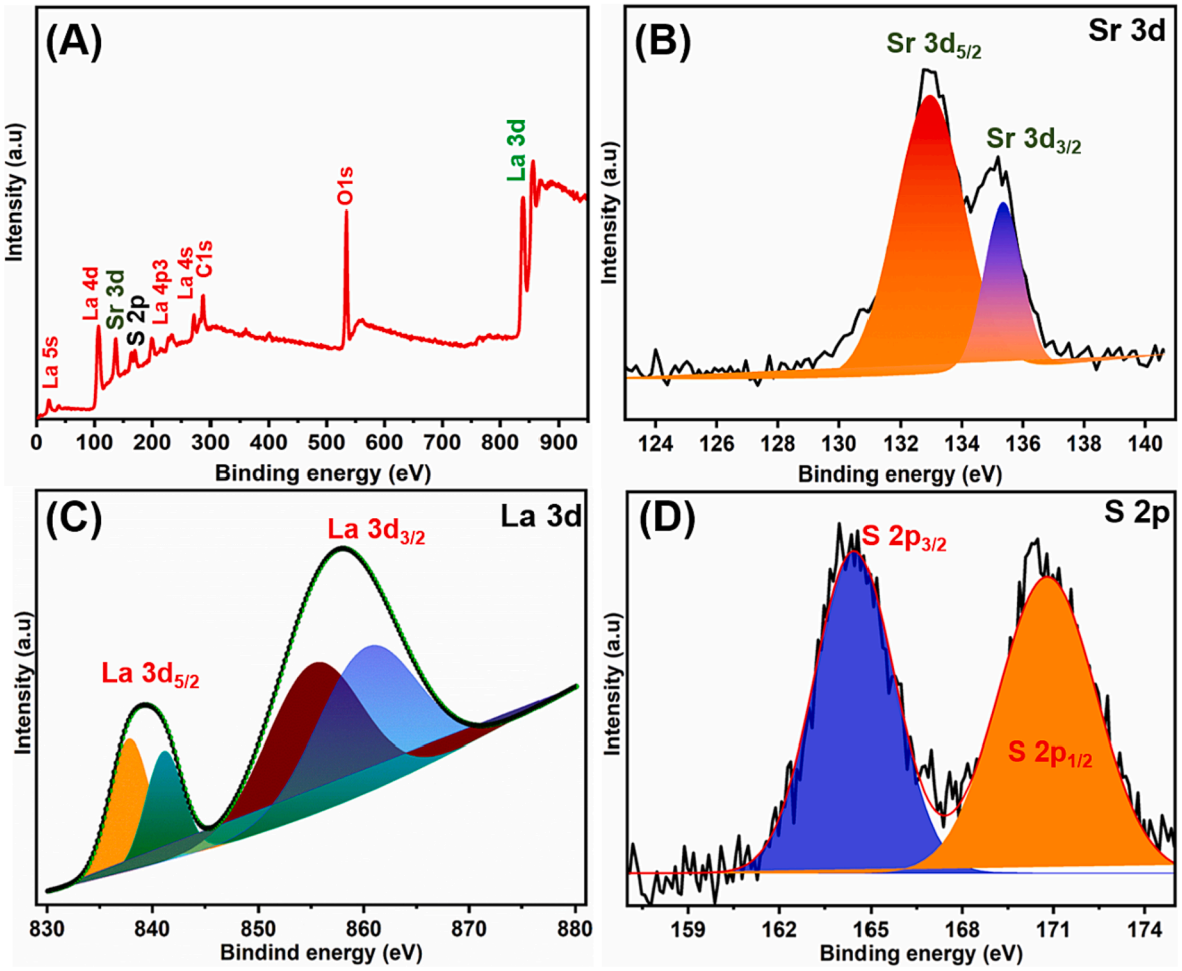

Fig. 2. XPS analysis of Sr@La_2S_3 (A), Sr 3d (B), La3d (C), S 2p (D).

(cm^2), diffusion coefficient (7.6×10^{-6}), response peak current, number of electrons in the electrochemical reactions, scan rate of the reaction in CV analysis (Vs^{-1}) and the concentration of the reaction molecules, respectively. Based on the Randles-Sevcik equation and obtained electrochemical parameters, the electrochemical active surface area (ECSA) was calculated. Moreover, more significant properties of ECSA for Sr@La_2S_3/GCE is 0.126 cm^2. To compare with other electrodes of La_2S_3/GCE (0.103 cm^2) and bare GCE (0.019 cm^2), the Sr doped La_2S_3 modified electrode has higher ECSA.

To find out the difference in the electrocatalytic performance of bare and modified GCE, cyclic voltammetry has been carried out. The CV of 100 μM MTO at bare GCE, La_2S_3/GCE and Sr@La_2S_3/GCE in 0.05 M PB (pH = 7) at a 50 mVs^{-1} scan rate is depicted in Fig. 5A. A negligible reduction peak (−0.74 V) was observed with 4.1 μA current response for bare GCE which indicates the unsuitability of GCE towards the detection of MTO. Upon modification of GCE with La_2S_2 reduction peak was observes at −0.76 V with current 13.2 μA shows its electrochemical behavior towards the detection of MTO. When Sr@La_2S_3/GCE is used as the electrode, a considerable decrease in the potential with enhanced current response was observed. The potential of Sr@La_2S_3/GCE for the detection of MTO was found to be −0.63 V with 23.6 μA current. This enhanced current and lowered peak potential of Sr@La_2S_3/GCE for the detection of MTO are due to the synergistic effect of Sr metal on La_2S_3 and its layered structure. The Sr@La_2S_3/GCE's enhanced surface area, conductivity and layered structure accompany the easy and swift mobility of electrons during the redox reaction of the MTO [14].

The electrochemical performance of the material is mainly dependent on the pH of the electrolyte. Fig. 5B, describes the effect of pH on the electrochemical behavior of Sr@La_2S_3/GCE in presence of MTO. The pH was varied from 1 to 11, the current density response of Sr@La_2S_3/GCE was linear from pH 1 to 7 and a decrease in the current response was observed after pH 7. Hence, pH 7 is set as optimum to carry out further studies. The corresponding linear plot is given in Fig. 5C which indicates the dependence of peak current with the potential with regression coefficient $R^2 = 0.995$. The mechanism of electro-reduction of MTO at 0.05 M PB in presence of Sr@La_2S_3/GCE is given in Scheme 3. The reduction of MTO takes place in two steps. Step A is a chemical reaction that involves the keto-enol tautomerism and forms the protonated enol form of MTO. Step B is an electrochemical reaction, where MTO undergoes irreversible reduction by gaining 4 electrons and $4H^+$ in 0.5 M PB solution [14].

To know the range of MTO sensing by Sr@La_2S_3/GCE, CV has been carried out in 0.05 M PB by varying the concentration of MTO. Fig. 6A, indicates the peak potential linear with the concentration i.e. upon rising the concentration the reduction peaks current increases with a slight shift in the peak towards more negative potential. A corresponding calibration graph is given Fig. 6B which follows the equation as $I = -0.1022$ μA μM^{-1} X-4.0779 ($R^2 = 0.9938$). Fig. 6C, indicates the plot of log concentration of MTO against log current, which is found to be linear with $R^2 = 0.9983$. CV of 100 μM MTO in presence of Sr@La_2S_3/GCE was recorded by varying the scan rate from 0.02 to 0.4 Vs^{-1} in 0.05 M PB solution (Fig. 6D). It is found that the current response was linear with the scan rate indicates the superior electrochemical behaviour of Sr@La_2S_3 towards the detection of MTO. The inset is a plot of the square root of the scan rate versus current shows the good linearity with the linear regression equation −29.468x-4.8805 with regression co-efficient

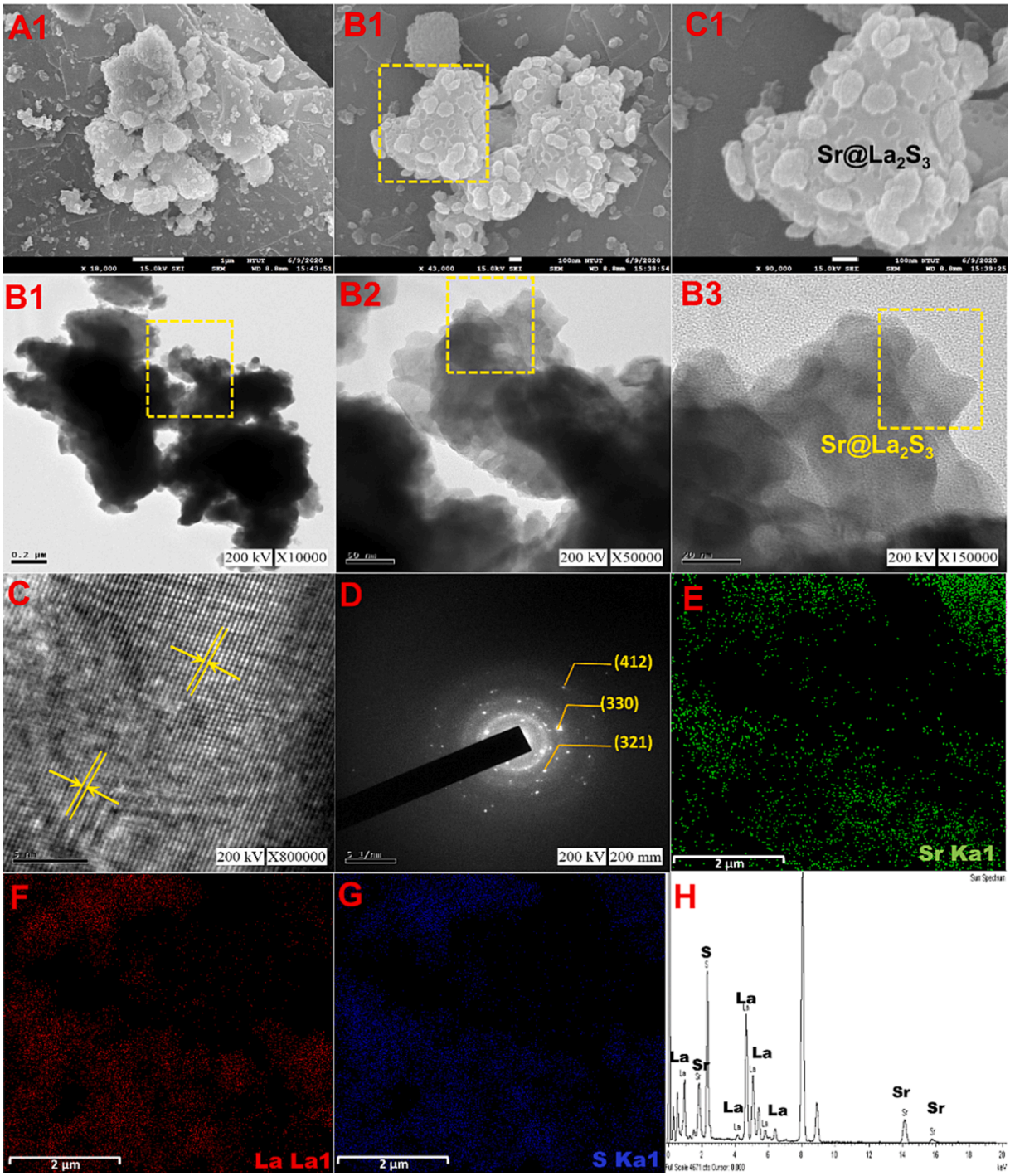

Fig. 3. SEM of $Sr@La_2S_3$ (A1-A3) and TEM analysis of $Sr@La_2S_3$ (B1-B3 and C). SAED pattern of $Sr@La_2S_3$ (D). Elemental mapping analysis of composite (E-G) and elemental analysis of $Sr@La_2S_3$ (H).

$R^2 = 0.9915$ (inset). This indicates the diffusion-controlled phenomena that occur during the electrochemical detection of MTO in presence of $Sr@La_2S_3$/GCE [41,42]. Fig. 6E is the calibration graph of log scan rate against potential, which is found to be linear with regression co-efficient value 0.9916. Another calibration curve (Fig. 6F) indicates the dependence of current on the applied potential. The current is linear with the applied potential with the R^2 value 0.9966.

3.4. Amperometric detection

$Sr@La_2S_3$/RDE has been further subjected to amperometric detection of different concentrations of MTO to find out the analytical parameters like sensitivity and limit of detection (LOD). Fig. 7A depicts the amperometric profile of MTO in 0.05 M of PB (pH = 7.0). With the increase in the addition of MTO has observed to increase the peak potential. A wide range of detection is observed with LOD of 2.4 nM [43–45]. Its corresponding calibration curve of different concentrations of MTO against the current is given in Fig. 7B. The reduction of MTO is linear with the increase in the concentration of MTO, still, a slight variation is observed in lower and higher concentrations of MTO. The linear regression equation at lower concentration (up to around 100 µM) equation Ip_c (µA) = 0.7322 µM – 1.9366 with 0.9948 R^2 value. At higher

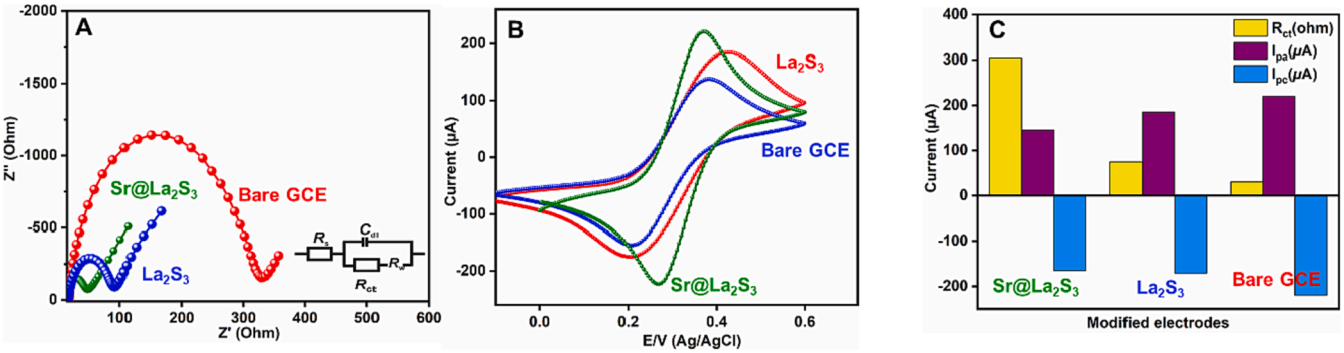

Fig. 4. (A) EIS and (B), CV analysis of unmodified GCE, La_2S_3/GCE, and Sr@La_2S_3/GCE in 5 mM $[Fe(CN)6)]^{3-/4-}$ containing 0.1 M of KCl as the electrolyte (inset: Randles circuit). (C), corresponding calibration plot.

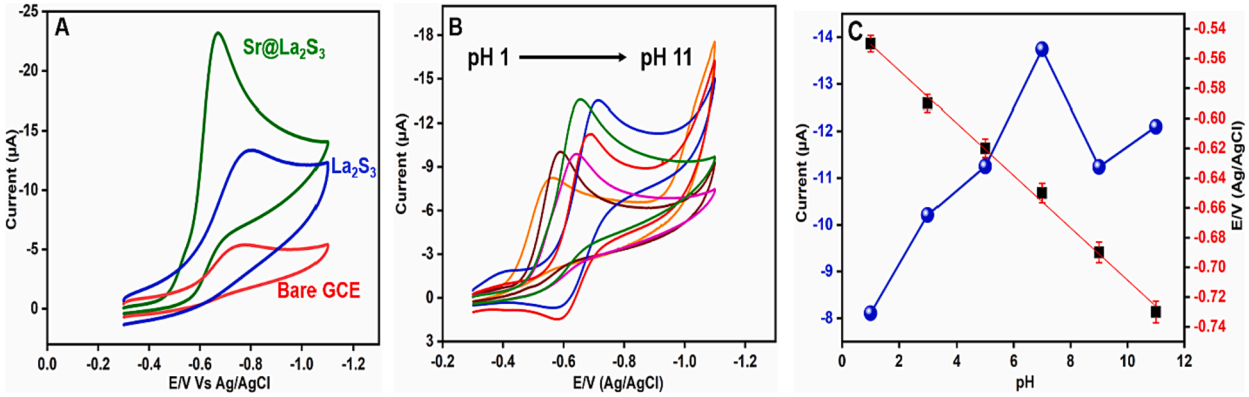

Fig. 5. (A) CV response for 100 μM MTO at bare GCE, La_2S_3/GCE and Sr@La_2S_3/GCE in 0.05 M PB (pH = 7) at a 50 mVs^{-1}scan rate. (B-C) pH analysis in Sr@La_2S_3/GCE with MTO.

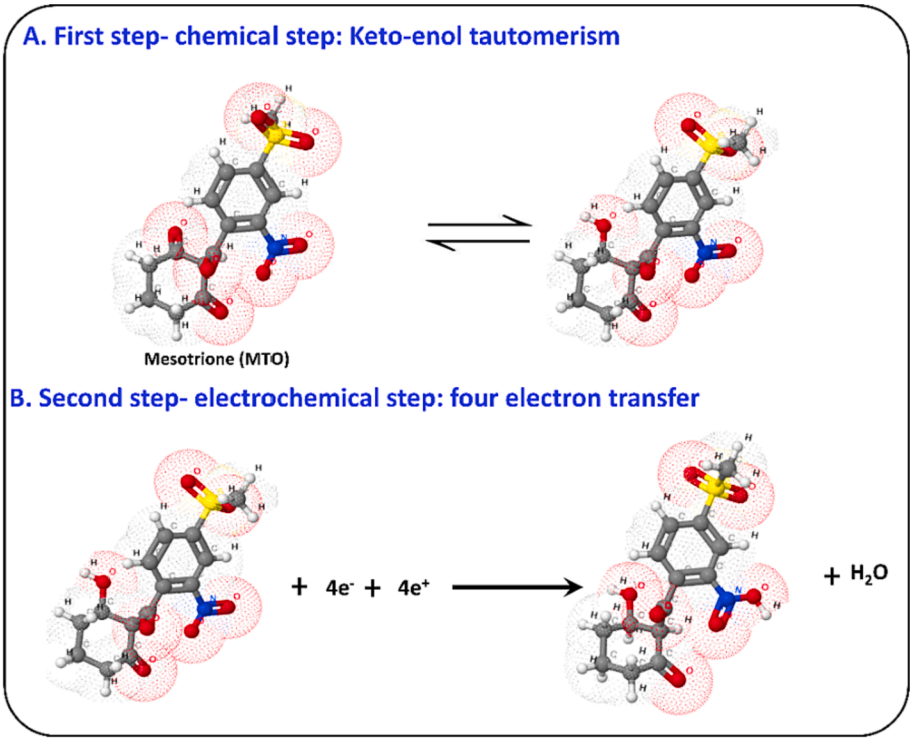

Scheme 3. Electrochemical reduction of MTO at Sr@La_2S_3 modified electrode in 0.05 M of PB (pH 7.0).

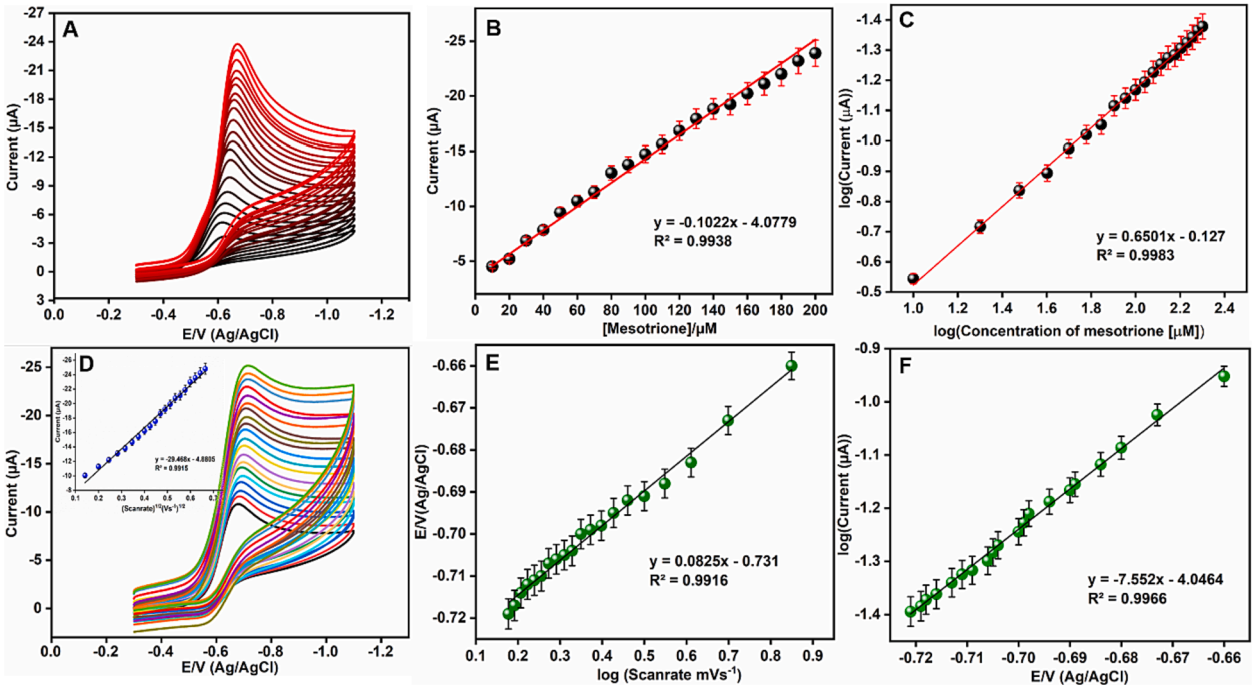

Fig. 6. (A) CV of Sr@La_2S_2/GCE at different quantities of MTO (10 to 200 μM) in 0.05 M PB (pH = 7.0) and (B-C) corresponding calibration plot. (D) CV platform of Sr@La_2S_3/GCE containing 100 μM MTO at different sweep rates 0.02–0.4 Vs^{-1} in 0.05 M of PB (pH = 7) and (E-F) corresponding linear calibration plots.

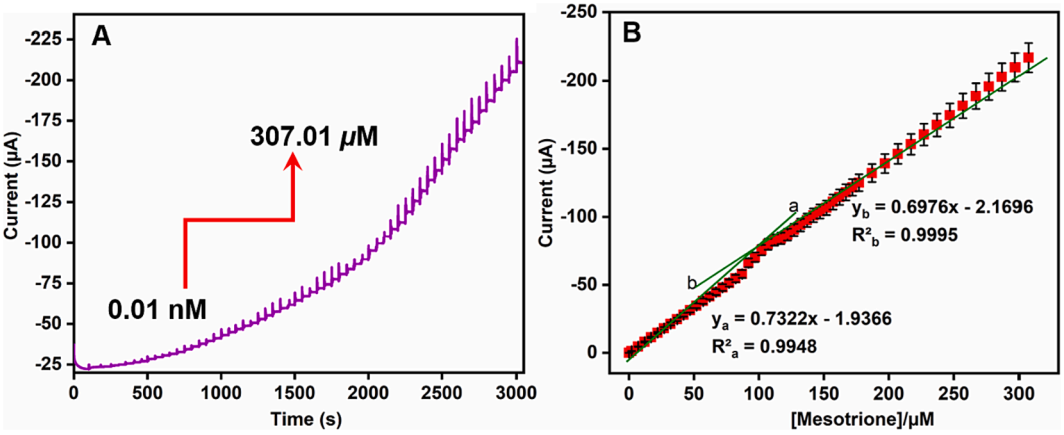

Fig. 7. (A) amperometric responses of Sr@La_2S_3/RDE at different quantities of MTO (0.01–307.01 μM) in 0.05 M of PB (RPM = 1200). (B) linear dependence for the concentration of MTO (μM) vs current (μA).

concentration of MTO (above 100 μM) the equation follows I_{pa} (μA) = 0.6976 μM – 2.1696 with 0.9995 R^2 value. This indicates, the amperometric approach is best suited in both higher and lower concentrations of MTO, which is a much-needed sensing characteristic of a material. The sensitivity of Sr@La_2S_2/RDE is very higher (40.677 & 38.755 $\mu A \cdot \mu M^{-1} \cdot cm^{-2}$) with a wide linear range (0.01–307.01 μM) and low LOD values indicate its superiority over different methods available in the literature by using various techniques towards the electrochemical

Table 1
Comparison of electrochemical parameters for the detection of MTO toxic chemical at Sr@La_2S_3 modified RDE with other research articles.

Electrode	Methods	Sensitivity ($\mu A \cdot \mu M^{-1} \cdot cm^{-2}$)	Linear range (μM)	LOD (nM)	Reference
Carbon/GCE	DPV	2.58	0.25–8.5	70	[20]
carbon quantum dots	MIFP	–	0.015 to 3.0	4.7	[16]
Organoclay/GCE	SWV	6.54	0.25–2.5	25	[46]
silver/amalgam electrode	DPV	–	0.10–10	50	[47]
carbon black/GCE	SWV	2.34	0.040–7.2	26	[48]
NfrA2@MgAl-NPs	AMP	18.4	5–60	300	[18]
Fe(III) complex	UV–vis	0.379	0.2–10.0	53	[19]
HPPD	CV	–	1–237	65	[49]
Sr@La_2S_3/RDE	AMP	40.677 & 38.755	0.01–307.1	2.4	This work

detection of MTO (Table 1). Moreover, limit of quantification is calculated as 10 nM in the modified sensor.

3.5. Interference studies

A stable sensor can detect the analyte even in the presence of other interferants. To find out the selectivity of Sr@La_2S_3/RDE towards the detection of MTO, interference studies have been carried out and are given in Fig. 8A. The current response Sr@La_2S_3/RDE in amperometric detection MTO (50 μM) in presence of various pharmaceutical drugs, biological analytes and metals (10-fold excess) are given in Fig. 8A-C, respectively. A clear response is observed only for MTO, the response for other analytes is very negligible and does not affect MTO response. The results indicate, Sr@La_2S_3/RDE is a selective electrode for sensing MTO in 0.05 M PB and can be detected even in the presence of organic and inorganic species along with analyte. Mainly, the possible reason for the selective detection of MTO is each interferents have specific potentials with adsorption sites on the surface of Sr@La_2S_3/RDE, while the adsorption of MTO could be remarkably higher compare to other analytes. The applied potential is drastically lowered which is one of the important reasons for selectivity.

The stability of the Sr@La_2S_3/RDE for the detection of MTO have been evaluated by carrying out the amperometric studies for 30 days (Fig. 8D). After the modification of Sr@La_2S_3/RDE was placed at 4 °C, when not in use. The Sr@La_2S_3/RDE is found to exhibit high stability with a constant current response even up to 30 days (more than 95 %). Further, MTO has been detected in different water samples and grape extract samples using Sr@La_2S_2/RDE by optimized amperometric method.

3.6. Real sample demonstration using Sr@La_2S_3 catalyst

In the real sample studies, we used the amperometric method at Sr@La_2S_3/RDE for analysis of MTO in industrial, river water and fruit extract samples. Based on the previous literature, MTO is contaminated in water resources and fruits. Real sample preparation is given in the supporting information. For the experiment, the obtained real samples were directly analyzed based on the optimized conditions. Furthermore, an MTO was spiked and prepared known concentration of real samples.

Table 2
Detection of MTO in water and fruit samples at Sr@La_2S_3 catalyst modified electrode.

sample	Added (nM)	Found (nM)	Recovery (%)	RSD/±% (n = 3)
Industrial water	0	0	–	–
	200	198.5	99.25	0.94
	500	496.2	99.24	0.59
River water	0	0	–	–
	200	197.9	98.95	1.02
	500	497.2	99.44	0.91
Fruit extract (grape)	0	0	–	–
	200	198.8	99.4	0.84
	500	498.1	99.62	0.69

The spiked real samples were tested and current response was observed using Sr@La_2S_3/RDE. Results for the recovery of MTO in the industrial, river water and fruit extract samples are shown in Table 2. As a result of the testing, Sr@La_2S_3 modified electrode appeared to have excellent capabilities for MTO detection in various real samples. The RSD values are less than 2 %, which indicates a very good selective detection of MTO not only with other species but also at the different environments of the analyte.

4. Conclusion

The work involves the simple one-pot hydrothermal synthetic method for the generation of layered strontium doped dilanthanum trisulfide. The electrocatalytic activities of the La_2S_3 and Sr@La_2S_3 have been used as modifiers on RDE. The electrocatalytic results indicate Sr@La_2S_3/RDE exhibit enhanced activity than La_2S_3/GCE for the detection of MTO chemical in 0.05 phosphate buffer. Results show that doping of Sr to La_2S_3 positively enhanced the electrochemical performance due to increased conductivity and active sites on the surface. The Sr@La_2S_3/GCE showed very good stability, sensitivity, and selectivity for MTO detection with a wide range and lower LOD values. This is the first report on metal-doped lanthanum sulfide for the detection of an herbicide. This report opens up the gate for the research on metal-doped lanthanum sulfides towards the detection of organic molecules in the chemical and pharmaceutical industries.

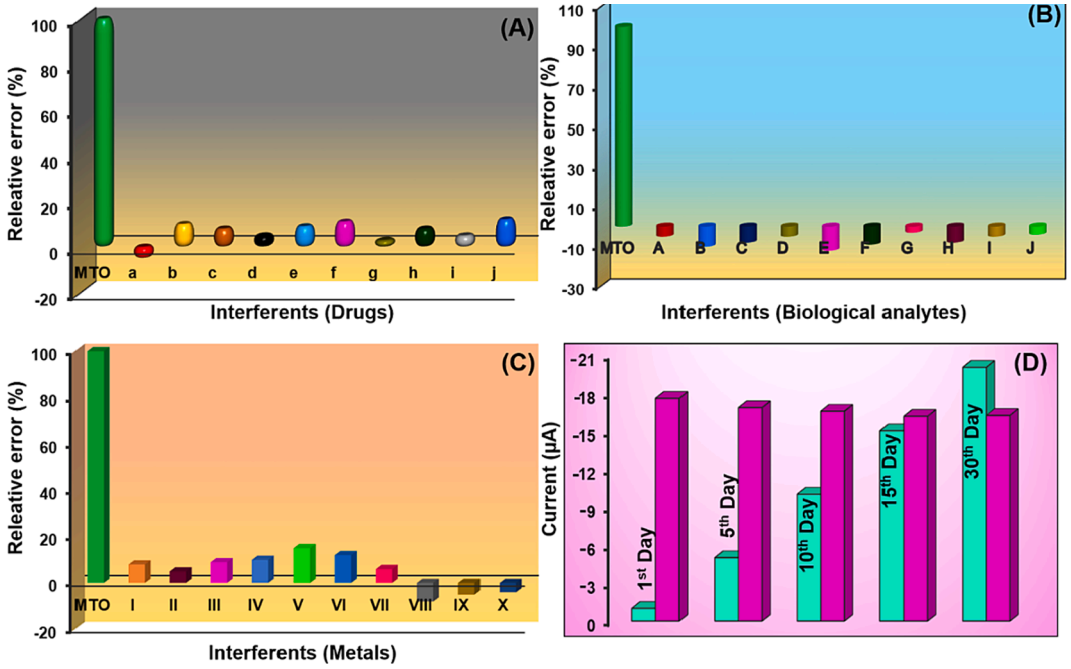

Fig. 8. (A-C) Interference analysis based on Sr@La_2S_2/RDE in 100 μM MTO and different interferences. (D) Stability analysis at Sr@La_2S_3/RDE in MTO.

CRediT authorship contribution statement

Umamaheswari Rajaji: Conceptualization, Formal analysis, Investigation, Writing – original draft. **K. Yogesh Kumar:** Validation, Writing – review & editing. **Rameshkumar Arumugam:** Data curation, Methodology. **Asma A. Alothman:** Writing – review & editing, Conceptualization. **Mohamed Ouladsmane:** Funding acquisition, Writing – review & editing. **Ren-Jei Chung:** Investigation, Supervision, Conceptualization. **Ting-Yu Liu:** Project administration, Supervision, Funding acquisition, Writing – original draft, Writing – review & editing.

Declaration of Competing Interest

The authors declare that they have no known competing financial interests or personal relationships that could have appeared to influence the work reported in this paper.

Acknowledgments

The authors gratefully acknowledge the financial support of the National Science and Technology Council of Taiwan (NSTC 111-2221-E-131-020-MY3, NSTC 110-2221-E-131-009, and NSTC 110-2622-E-131-005) and Research Center for Intelligent Medical Devices of Ming Chi University of Technology, Taiwan. This work was funded by the Researchers Supporting Project Number (RSP-2021/243) King Saud University, Riyadh, Saudi Arabia.

Appendix A. Supplementary data

Supplementary data to this article can be found online at https://doi.org/10.1016/j.ultsonch.2022.106251.

References

[1] M. Ashokkumar, The characterization of acoustic cavitation bubbles–an overview, Ultrason. Sonochem. 18 (2011) 864–872.
[2] M. Govindasamy, S.-F. Wang, A. Almahri, U. Rajaji, Effects of sonochemical approach and induced contraction of core–shell bismuth sulfide/graphitic carbon nitride as an efficient electrode materials for electrocatalytic detection of antibiotic drug in foodstuffs, Ultrason. Sonochem. 72 (2021), 105445.
[3] T.-W. Chen, U. Rajaji, S.-M. Chen, M. Govindasamy, S.S.P. Selvin, S. Manavalan, R. Arumugam, Sonochemical synthesis of graphene oxide sheets supported Cu2S nanodots for high sensitive electrochemical determination of caffeic acid in red wine and soft drinks, Compos. B Eng. 158 (2019) 419–427.
[4] J. Theerthagiri, J. Madhavan, S.J. Lee, M.Y. Choi, M. Ashokkumar, B.G. Pollet, Sonoelectrochemistry for energy and environmental applications, Ultrason. Sonochem. 63 (2020) 104960.
[5] A. Muthumariyappan, U. Rajaji, S.-M. Chen, N. Baskaran, T.-W. Chen, R. J. Ramalingam, Sonochemical synthesis of perovskite-type barium titanate nanoparticles decorated on reduced graphene oxide nanosheets as an effective electrode material for the rapid determination of ractopamine in meat samples, Ultrason. Sonochem. 56 (2019) 318–326.
[6] V.J. Mane, S.B. Kale, S.B. Ubale, V.C. Lokhande, U.M. Patil, C.D. Lokhande, Lanthanum sulfide-manganese sulfide/graphene oxide (La2S3-MnS/GO) composite thin film as an electrocatalyst for oxygen evolution reactions, J. Solid State Electrochem. 25 (2021) 1775–1788.
[7] H. Peng, H. Wang, L. Wang, C. Huang, X. Zheng, J. Wen, Efficient adsorption-photocatalytic removal of tetracycline hydrochloride over La2S3-modified biochar with S, N-codoping, J. Water Process Eng. 49 (2022) 103038.
[8] M. Govindasamy, S.-F. Wang, W.C. Pan, B. Subramanian, R.J. Ramalingam, H. Al-Lohedan, Facile sonochemical synthesis of perovskite-type SrTiO3 nanocubes with reduced graphene oxide nanocatalyst for an enhanced electrochemical detection of α-amino acid (tryptophan), Ultrason. Sonochem. 56 (2019) 193–199.
[9] Y. Li, A Study on the Consolidation of Sulfide-based Infrared Optical Ceramics, Alfred University, 2019.
[10] H. Li, X. Ren, P. Xi, H. Huang, C. Zhang, F. Luo, Influence of NaX (X= Cl, Br, I) additive on phase composition, thermostability and high infrared performances of γ-La2S3 transparent ceramics, Ceram. Int. 46 (2020) 9145–9153.
[11] M. van Dijk, T. Morley, M.L. Rau, Y. Saghai, A meta-analysis of projected global food demand and population at risk of hunger for the period 2010–2050, Nature Food 2 (7) (2021) 494–501.
[12] A.A. Lahcen, S.G. Surya, T. Beduk, M.T. Vijjapu, A. Lamaoui, C. Durmus, S. Timur, O. Shekhah, V. Mani, A. Amine, Metal–Organic Frameworks Meet Molecularly Imprinted Polymers: Insights and Prospects for Sensor Applications, ACS Appl. Mater. Interfaces (2022).
[13] P. Arul, S.-T. Huang, V. Mani, Y.-C. Hu, Ultrasonic synthesis of bismuth-organic framework intercalated carbon nanofibers: A dual electrocatalyst for trace-level monitoring of nitro hazards, Electrochim. Acta 381 (2021) 138280.
[14] U. Rajaji, S. Chinnapaiyan, S.-M. Chen, M. Govindasamy, J.I.d. Oliveira Filho, W. Khushaim, V. Mani, Design and fabrication of yttrium ferrite garnet-embedded graphitic carbon nitride: a sensitive electrocatalyst for smartphone-enabled point-of-care pesticide (mesotrione) analysis in food samples, ACS Appl. Mater. Interfaces 13 (21) (2021) 24865–24876.
[15] Y. Liu, L.u. Li, M. Yue, L. Yang, F. Sun, G. Xu, Y. Fu, F. Ye, A Switch-On fluorescent probe for detection of mesotrione based on the straightforward cleavage of carbon-nitrogen double bond of Schiff base, Chem. Eng. J. 430 (2022) 132758.
[16] X. Sun, Y. Liu, N. Niu, L. Chen, Synthesis of molecularly imprinted fluorescent probe based on biomass-derived carbon quantum dots for detection of mesotrione, Anal. Bioanal. Chem. 411 (2019) 5519–5530.
[17] B.K. Doan, C.H. Nguyen, T.T. Bui, T.V. Tran, H.P. Huynh, Q.-T. Nguyen, S.T. Cu, L.-T.-T. Nguyen, C.D. Tran, P.T. Mai, Synthesis of Conjugated Molecules Based on Dithienopyrrole Derivatives and Pyrene as Chemosensor for Mesotrione Detection, J. Braz. Chem. Soc. 33 (2022) 1106–1116.
[18] S. Hdiouech, F. Bruna, I. Batisson, P. Besse-Hoggan, V. Prevot, C. Mousty, Amperometric detection of the herbicide mesotrione based on competitive reactions at nitroreductase@ layered double hydroxide bioelectrode, J. Electroanal. Chem. 835 (2019) 324–328.
[19] M. Muhammad, S. Khan, H. Fayaz, Charge-transfer complex–based spectrophotometric method for the determination of mesotrione in environmental samples, Environ. Monit. Assess. 193 (2021) 1–7.
[20] H. Barchanska, P. Markowski, M. Strzebin, Electrochemical determination of mesotrione and its degradation products on glassy carbon electrode, Int. J. Environ. Anal. Chem. 98 (2018) 493–505.
[21] D. Šojić Merkulov, M. Lazarević, A. Djordjevic, M. Náfrádi, T. Alapi, P. Putnik, Z. Rakočević, M. Novaković, B. Miljević, S. Bognár, B. Abramović, Potential of TiO2 with various Au nanoparticles for catalyzing mesotrione removal from wastewaters under sunlight, Nanomaterials 10 (8) (2020) 1591.
[22] M. Govindasamy, S. Sakthinathan, S.-M. Chen, T.-W. Chiu, A. Sathiyan, J.P. Merlin, Reduced graphene oxide supported cobalt Bipyridyl complex for sensitive detection of methyl parathion in fruits and vegetables, Electroanalysis 29 (8) (2017) 1950–1960.
[23] S. Sakthinathan, S. Kubendhiran, S.-M. Chen, M. Govindasamy, F.M.A. Al-Hemaid, M. Ajmal Ali, P. Tamizhdurai, S. Sivasanker, Metallated porphyrin noncovalent interaction with reduced graphene oxide-modified electrode for amperometric detection of environmental pollutant hydrazine, Appl. Organomet. Chem. 31 (9) (2017) e3703.
[24] S. Manavalan, U. Rajaji, S.-M. Chen, S. Steplin Paul Selvin, M. Govindasamy, T.-W. Chen, M. Ajmal Ali, F.M.A. Al-Hemaid, M.S. Elshikh, Determination of 8-hydroxy-2′-deoxyguanosine oxidative stress biomarker using dysprosium oxide nanoparticles@ reduced graphene oxide, Inorg. Chem. Front. 5 (11) (2018) 2885–2892.
[25] S. Chinnapaiyan, H.T. Das, S.-M. Chen, M. Govindasamy, R.A. Alshgari, C.-H. Fan, C.-H. Huang, CoAl2O4 nanoparticles modified carbon nanofibers as high-efficiency bifunctional electrocatalyst: An efficient electrochemical aqueous asymmetric supercapacitors and non-enzymatic electrochemical sensors, J. Alloy. Compd. 931 (2023) 167553.
[26] M. Govindasamy, C.-R. Jian, C.-F. Kuo, A.-H. Hsieh, J.-L. Sie, C.-H. Huang, A chemiresistive biosensor for detection of cancer biomarker in biological fluids using CVD-grown bilayer graphene, Microchim. Acta 189 (2022) 1–12.
[27] S. Vinoth, M. Govindasamy, S.-F. Wang, Solvothermal synthesis of silver tungstate integrated with carbon nitrides matrix composites for highly sensitive electrochemical nitrofuran derivative sensing in biological samples, Anal. Chim. Acta 1192 (2022) 339355.
[28] V. Mani, C. Durmus, W. Khushaim, D.C. Ferreira, S. Timur, F. Arduini, K.N. Salama, Multiplexed sensing techniques for cardiovascular disease biomarkers-A review, Biosens. Bioelectron. 216 (2022) 114680.
[29] W. Khushaim, V. Mani, K. Peramaiya, K.-W. Huang, K.N. Salama, Ruthenium and Nickel Molybdate-Decorated 2D Porous Graphitic Carbon Nitrides for Highly Sensitive Cardiac Troponin Biosensor, Biosensors 12 (2022) 783.
[30] M.W. Raza, S. Kiran, A. Razaq, M.F. Iqbal, A. Hassan, S. Hussain, M.N. Ashiq, Z. Meng, Strategy to enhance the electrochemical characteristics of lanthanum sulfide nanorods for supercapacitor applications, J. Nanopart. Res. 23 (2021) 1–12.
[31] Z. Zhu, Y. Yang, Y. Fan, L. Zhang, S. Tang, Y. Zhu, X. Zhou, Strontium-doped hydroxyapatite as an efficient adsorbent for Cd (II) removal from wastewater: Performance, kinetics, and mechanism, Environ. Technol. Innov. 28 (2022) 102575.
[32] R. Savari, J. Rouhi, O. Fakhar, S. Kakooei, D. Pourzadeh, O. Jahanbakhsh, S. Shojaei, Development of photo-anodes based on strontium doped zinc oxide-reduced graphene oxide nanocomposites for improving performance of dye-sensitized solar cells, Ceram. Int. 47 (2021) 31927–31939.
[33] Y. Ji, M. Wang, Z. Yang, H. Wang, M.A. Padhiar, H. Qiu, J. Dang, Y. Miao, Y. Zhou, A.S. Bhatti, Strong violet emission from ultra-stable strontium-doped CsPbCl 3 superlattices, Nanoscale 14 (2022) 2359–2366.
[34] Y. Pang, X. Zhou, E.I. Vovk, C. Guan, S. Li, A.P. van Bavel, Y. Yang, Understanding lanthanum oxide surface structure by DFT simulation of oxygen 1s calibrated binding energy in XPS after in situ treatment, Appl. Surf. Sci. 548 (2021) 149214.
[35] K. Tang, C. An, P. Xie, G. Shen, Y. Qian, Low-temperature synthesis and characterization of β-La2S3 nanorods, J. Cryst. Growth 245 (2002) 304–308.
[36] M. Govindasamy, S.-M. Chen, V. Mani, R. Devasenathipathy, R. Umamaheswari, K. J. Santhanaraj, A. Sathiyan, Molybdenum disulfide nanosheets coated multiwalled carbon nanotubes composite for highly sensitive determination of chloramphenicol

in food samples milk, honey and powdered milk, J. Colloid Interface Sci. 485 (2017) 129–136.
[37] M. Govindasamy, R. Umamaheswari, S.-M. Chen, V. Mani, C. Su, Graphene oxide nanoribbons film modified screen-printed carbon electrode for real-time detection of methyl parathion in food samples, J. Electrochem. Soc. 164 (9) (2017) B403–B408.
[38] A. Muthumariappan, M. Govindasamy, S.-M. Chen, K. Sakthivel, V. Mani, Screen-printed electrode modified with a composite prepared from graphene oxide nanosheets and Mn3O4 microcubes for ultrasensitive determination of nitrite, Microchim. Acta 184 (9) (2017) 3625–3634.
[39] V. Mani, M. Govindasamy, S.-M. Chen, T.-W. Chen, A.S. Kumar, S.-T. Huang, Core-shell heterostructured multiwalled carbon nanotubes@ reduced graphene oxide nanoribbons/chitosan, a robust nanobiocomposite for enzymatic biosensing of hydrogen peroxide and nitrite, Sci. Rep. 7 (2017) 1–10.
[40] U. Rajaji, M. Govindasamy, R. Sha, R.A. Alshgari, R.-S. Juang, T.-Y. Liu, Surface engineering of 3D spinel Zn3V2O8 wrapped on sulfur doped graphitic nitride composites: Investigation on the dual role of electrocatalyst for simultaneous detection of antibiotic drugs in biological fluids, Compos. B Eng. 242 (2022) 110017.
[41] U. Rajaji, P.-S. Ganesh, S.-Y. Kim, M. Govindasamy, R.A. Alshgari, T.-Y. Liu, MoS2 Sphere/2D S-Ti3C2 MXene Nanocatalysts on Laser-Induced Graphene Electrodes for Hazardous Aristolochic Acid and Roxarsone Electrochemical Detection, ACS Appl. Nano Mater. 5 (3) (2022) 3252–3264.
[42] S. Chinnapaiyan, U. Rajaji, S.-M. Chen, T.-Y. Liu, J.I. de Oliveira Filho, Y.-S. Chang, Fabrication of thulium metal–organic frameworks based smartphone sensor towards arsenical feed additive drug detection: Applicable in food safety analysis, Electrochim. Acta 401 (2022) 139487.
[43] T.-W. Chen, U. Rajaji, S.-M. Chen, R.J. Ramalingam, A relative study on sonochemically synthesized mesoporous WS2 nanorods & hydrothermally synthesized WS2 nanoballs towards electrochemical sensing of psychoactive drug (Clonazepam), Ultrason. Sonochem. 54 (2019) 79–89.
[44] U. Rajaji, T.-W. Chen, S. Chinnapaiyan, S.-M. Chen, M. Govindasamy, Two-dimensional binary nanosheets (Bi2Te3@ g-C3N4): application toward the electrochemical detection of food toxic chemical, Anal. Chim. Acta 1125 (2020) 220–230.
[45] U. Rajaji, S.V. Selvi, S.-M. Chen, S. Chinnapaiyan, T.-W. Chen, M. Govindasamy, A nanocomposite consisting of cuprous oxide supported on graphitic carbon nitride nanosheets for non-enzymatic electrochemical sensing of 8-hydroxy-2′-deoxyguanosine, Microchim. Acta 187 (2020) 1–10.
[46] J.K. Wagheu, C. Forano, P. Besse-Hoggan, I.K. Tonle, E. Ngameni, C. Mousty, Electrochemical determination of mesotrione at organoclay modified glassy carbon electrodes, Talanta 103 (2013) 337–343.
[47] M. Jovic, D. Manojlovic, D. Stankovic, A. Milic, M. Sentic, G. Roglic, Volta metric behavior of mesotrione using silver/amalgam electrode, (2013).
[48] P.B. Deroco, B.C. Lourencao, O. Fatibello-Filho, The use of modified electrode with carbon black as sensor to the electrochemical studies and voltammetric determination of pesticide mesotrione, Microchem. J. 133 (2017) 188–194.
[49] P.S. Garcia, A.L.D. Moreau, J.C.M. Ierich, A.C.A. Vig, A.M. Higa, G.S. Oliveira, F. C. Abdalla, M. Hausen, F.L. Leite, A nanobiosensor based on 4-hydroxyphenyl-pyruvate dioxygenase enzyme for mesotrione detection, IEEE Sens. J. 15 (2014) 2106–2113.